11-2009

Fragmentation Properties of Three-membered Ring Heterocyclic Molecules by Partial Ion Yield Spectroscopy: C2H4O and C2H4S

Wayne C. Stolte
University of Nevada, Las Vegas, wcstolte@lbl.gov

I. Dumitriu
Western Michigan University

S-W Yu
Lawrence Livermore National Laboratory

Gunnar Ohrwall
MAX-lab, Lund University

Maria Novella Piancastelli
Uppsala University, maria-novella.piancastelli@physics.uu.se

Fragmentation properties of three-membered heterocyclic molecules by partial ion yield spectroscopy: C2H4O and C2H4S

W. C. Stolte, I. Dumitriu, S.-W. Yu, G. Öhrwall, M. N. Piancastelli et al.

Citation: J. Chem. Phys. **131**, 174306 (2009); doi: 10.1063/1.3257685
View online: http://dx.doi.org/10.1063/1.3257685
View Table of Contents: http://jcp.aip.org/resource/1/JCPSA6/v131/i17
Published by the American Institute of Physics.

Fragmentation properties of three-membered heterocyclic molecules by partial ion yield spectroscopy: C_2H_4O and C_2H_4S

W. C. Stolte,[1,2,a)] I. Dumitriu,[3] S.-W. Yu,[4] G. Öhrwall,[5] M. N. Piancastelli,[6] and D. W. Lindle[1]
[1]*Department of Chemistry, University of Nevada, Las Vegas, Nevada 89154-4003, USA*
[2]*Advanced Light Source, Lawrence Berkeley National Laboratory, Berkeley, California 94720, USA*
[3]*Department of Physics, Western Michigan University, Kalamazoo, Michigan 49008-5252, USA*
[4]*Lawrence Livermore National Laboratory, Livermore, California 94550, USA*
[5]*MAX-lab, Lund University, Box 118, Lund SE-221 00, Sweden*
[6]*Department of Physics and Materials Science, Uppsala University, Box 530, Uppsala SE-751 21, Sweden*

(Received 17 July 2009; accepted 10 October 2009; published online 3 November 2009)

We investigated the photofragmentation properties of two three-membered ring heterocyclic molecules, C_2H_4O and C_2H_4S, by total and partial ion yield spectroscopy. Positive and negative ions have been collected as a function of photon energy around the C 1*s* and O 1*s* ionization thresholds in C_2H_4O, and around the S 2*p* and C 1*s* thresholds in C_2H_4S. We underline similarities and differences between these two analogous systems. We present a new assignment of the spectral features around the C *K*-edge and the sulfur $L_{2,3}$ edges in C_2H_4S. In both systems, we observe high fragmentation efficiency leading to positive and negative ions when exciting these molecules at resonances involving core-to-Rydberg transitions. The system, with one electron in an orbital far from the ionic core, relaxes preferentially by spectator Auger decay, and the resulting singly charged ion with two valence holes and one electron in an outer diffuse orbital can remain in excited states more susceptible to dissociation. A state-selective fragmentation pattern is analyzed in C_2H_4S which leads to direct production of S^{2+} following the decay of virtual-orbital excitations to final states above the double-ionization threshold. © *2009 American Institute of Physics*.
[doi:10.1063/1.3257685]

I. INTRODUCTION

After the creation of a core hole by an incident photon in a molecule composed of light atoms, valence electrons, which form the chemical bonds, are ejected from the molecule via the dominating Auger process, and the molecule usually dissociates into fragments, ions and/or neutrals. This is the basic process of photofragmentation.[1] In order to understand such photofragmentation processes in more detail it is useful to consider the regions below and above the ionization threshold separately. Below the threshold, following the excitation of a core electron to a bound unoccupied molecular orbital, a core hole decays via resonant Auger processes.[2,3] After resonant Auger decay, which typically produces singly ionized states, the molecule is often unstable and dissociates into small ionic or neutral fragments. Above the ionization threshold, normal Auger decay dominates, yielding a doubly charged ion that is even more likely to dissociate.

Compared to photoabsorption or absorptionlike measurements, such as total-electron or total-ion yield (including near-edge x-ray-absorption fine structure for gas-phase and adsorbed species), there is a clear advantage in monitoring a channel that is highly selective with respect to different types of resonances. Moreover, our experimental apparatus possesses the unique capability to detect either positively charged species (cations) or negatively charged species (anions). Partial anion yield is more selective than other single-channel measurements. Recently, we applied anion-yield spectroscopy to a number of small molecules, and it has proven to be a selective probe of molecular core-level processes, providing unique experimental verification of shape resonances[4–6] and identifying specific bond-breaking processes in methanol.[7]

The selection of one particular fragment on a large photon energy range has the advantage to make it possible to emphasize transitions usually hidden (i.e., when ions are not selected in mass and charge) by one or several electronic states with high absorption cross section. The most striking example is the description, thanks to the measurement of negative ions, of doubly excited states above the direct ionization thresholds of the C 1*s* and O 1*s* core orbitals of CO,[4] the two nonequivalent N 1*s* orbitals of N_2O (Ref. 8) and O 1*s* of CO_2,[6] usually concealed by shape resonances.

Another interesting finding, which we observe in both of these systems, is derived from partial ion yield spectroscopy, the assessment that below threshold the relative intensities of spectral features related to core-to-Rydberg excitations increase as the fragmentation process is more extended. In other words, for the smaller fragments, the Rydberg states are much more prominent than for the parent molecular ions. This is directly related to spectator decay having a higher probability following excitation to the diffuse Rydberg orbitals, and many or most of the final two hole/one-particle states are dissociative.[9,10] We observe the same phenomenon

a)Electronic mail: wcstolte@lbl.gov.

in both the cation and the anion yields for these two molecules, and we attribute it to the same origin, confirming our previous observations.

The present experimental work examines three-membered ring heterocyclic systems, namely, C_2H_4O and C_2H_4S. Three-membered ring compounds have been of great interest to chemists since the discovery of the easy cleavage of cyclopropane single bonds, which was shown to be due to the strain related to the triangular structure. Furthermore, such high degree of strain in these compounds confers upon them properties similar to those of unsaturated compounds. Therefore, the electronic structure and dynamical behavior of ethylene oxide and ethylene sulfide, as prototype heterocyclic three-member ring systems, are of interest not only for fundamental studies but also for investigation of many applied chemical and physical phenomena.

The photodissociation of ethylene sulfide in the ultraviolet regime has been studied by several experiments,[11–14] but no photofragmentation studies are available involving core excitation. The absorption properties of C_2H_4O around both the C *K*-edge and the O *K*-edge have been investigated by inner-shell electron energy loss (ISEELS) spectroscopy.[15] To the best of our knowledge, no such experiments have been reported for C_2H_4S. Therefore, we reinvestigated the oxygen-containing heterocycle with total ion yield (TIY) with an improved resolution as compared to the literature data set, and we obtained additional information by measuring partial ion yields for all detectable fragments at both the C and the O *K* edges. We then extended the results to help interpret some of the spectral features for the sulfur-containing heterocycle. On the grounds of such analogy, we present a new assignment of the spectral features around the C *K*-edge and the sulfur $L_{2,3}$ edges, together with a detailed analysis of the various fragmentation patterns.

We observe the signature of postcollision interaction (PCI) effects in some of the cation yields in C_2H_4O above the O *K* edge. A peculiar fragmentation pathway in C_2H_4S leading to S^{2+} is identified and discussed, namely, a state-selective fragmentation pattern leading to the direct production of S^{2+} following the decay of virtual-orbital excitations to final states above the double-ionization threshold.

II. EXPERIMENTAL TECHNIQUE

Experiments were performed on beamline 8.0.1.3 at the Advanced Light Source, Lawrence Berkeley National Laboratory. The monochromator calibration near the sulfur $L_{2,3}$ edges was performed by comparison to the high-resolution photoabsorption measurement on H_2S by Hudson *et al.*[16] Based on our previous measurements on H_2S,[17] the resolution was estimated as 60 meV. Calibration near the C *K* edge was based on comparison to the Rydberg-state energy data of Prince *et al.*,[18] and electron-energy-loss measurements of Tronc *et al.*,[19] with a resolution of 150 meV, based on our previous measurements on CO_2.[6] Finally, the calibration and resolution (300 meV) estimated near the O *K* edge are based on high-resolution photoabsorption measurements on O_2 by Domke *et al.*[20]

Ion mass and charge characterization was done with a 180° hemispherical analyzer with a resolution of 1 mass in 50 amu.[21] Briefly, the fragments are created by interaction with the light beam at the exit of an effusive gas jet. Ions are extracted from the gas cell by an electric field and focused on the entrance slit of the analyzer by an electrostatic lens. They are then deflected between the plates of the analyzer and refocused onto the exit slit before being detected by a channel electron multiplier. The potentials of the analyzer electrodes can be tuned and/or switched in polarity to select fragments with a specific mass and charge. Great care was made during the adjustment of the magnetic mass spectrometer during the measurement process to ensure we were on top of the proper peak in the mass spectrum. The percentage of fragmentation for each ion with respect to the measured total-ion-yield was estimated by summing all of the individual partial-ion-yields to obtain a summed yield. This sum yield compared very favorably with the measured total yield, differing only by an overall constant collection efficiency factor. In a smooth structureless region, we then compared each individual partial yield with the sum yield to obtain the percentage of fragmentation. These should not be considered as absolute branching ratios; they are included to give the reader a feeling for the intensity differences between the various ion fragments, with an approximate error of 20%.

The working pressure in the target chamber was set to approximately 1×10^{-5} Torr and the chamber was isolated from the beamline vacuum by differential pumping. The two chemicals were commercially obtained, ethylene oxide as a 2% concentration mix with helium from Airgas, and ethylene sulfide as a 99% pure liquid from Sigma Aldrich. The ethylene sulfide sample was purged of contaminants by performing three freeze/thaw cycles while pumping out the excess vapors from the frozen sample with a mechanical pump. It was subsequently introduced into the chamber using its vapor pressure. The ethylene oxide was introduced directly as a gas through a separate gas manifold.

III. RESULTS

A. C_2H_4O: C *K*-edge

We have obtained absorption spectra in the TIY mode for C_2H_4O in the photon-energy region 282–340 eV, including the C 1*s* ionization threshold located at 292.91 eV. The TIY scans are reported in all figures for sake of comparison. The TIY has been energy calibrated by the values reported in Ref. 18 and agrees well with the ISEELS measurements of Szel and Brion.[15]

We detected an abundance of positively charged and negatively charged ions, and we measured partial ion yield spectra for all detected fragments. Most of those are reported in Figs. 1–6. The list of positively charged fragments (cations) includes: (i) the singly charged species $C_2H_4O^+$, $C_2H_3O^+$, $C_2H_2O^+$, C_2HO^+, and C_2O^+, shown in Fig. 1; CH_3O^+, CH_2O^+, CHO^+, and CO^+, shown in Fig. 2; $C_2H_3^+$, $C_2H_2^+$, C_2H^+, and C_2^+, shown in Fig. 3; CH_3^+, CH_2^+, CH^+, and C^+, shown in Fig. 4; (ii) the doubly charged species $C_2H_3O^{2+}$, $C_2H_2O^{2+}$, and C_2HO^{2+}, shown in Fig. 5. We also detected the singly charged fragments H^+, H_2^+, H_3^+, O^+, OH^+, and H_2O^+, and the doubly charged species $C_2H_3^{2+}$,

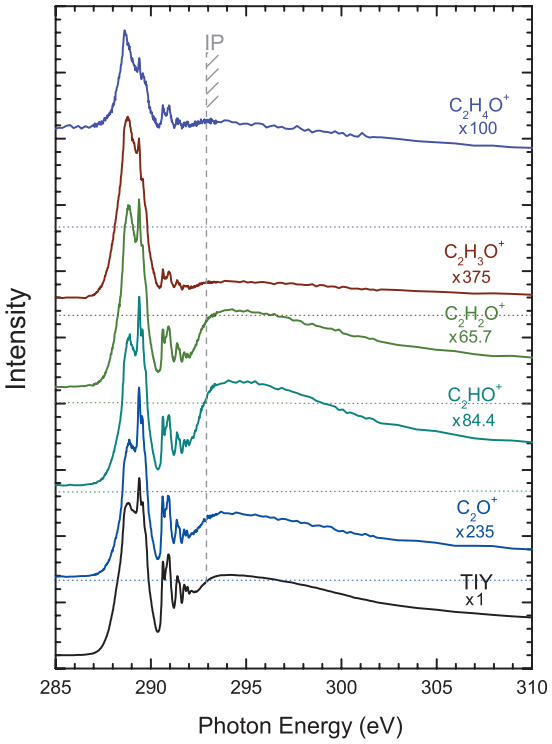

FIG. 1. Partial yields for $C_2H_4O^+$, $C_2H_3O^+$, $C_2H_2O^+$, C_2HO^+, and C_2O^+ ion fragments (cations) following photoexcitation of C_2H_4O near the C 1*s* ionization threshold, the TIY is added for comparison. Numerical values are approximate intensity values relative to the TIY at 295 eV.

$C_2H_2^{2+}$, C_2H^{2+}, CHO^{2+}, and C^{2+}, whose yields are not shown here, because they do not provide further information since they are either similar to other partial ion yields or simply mimic the TIY. The negatively charged species (anions) H^-, C^-, and O^- are shown in Fig. 6.

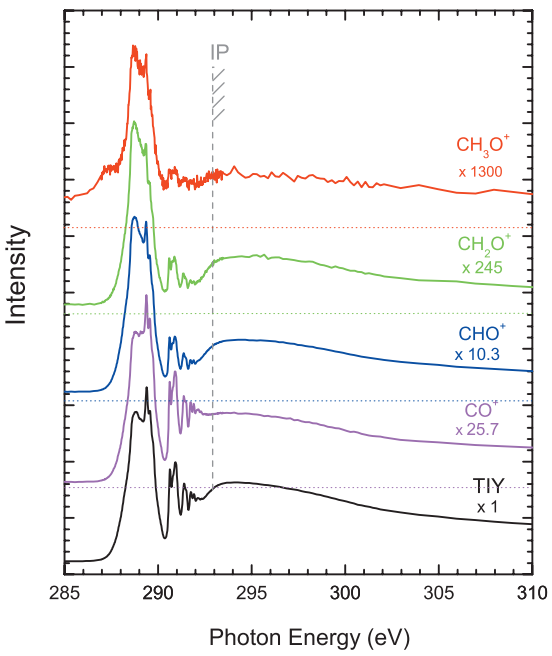

FIG. 2. Partial yields for CH_3O^+, CH_2O^+, CHO^+, and CO^+ ion fragments (cations) following photoexcitation of C_2H_4O near the C 1*s* ionization threshold, the TIY is added for comparison. Numerical values are approximate intensity values relative to the TIY at 295 eV.

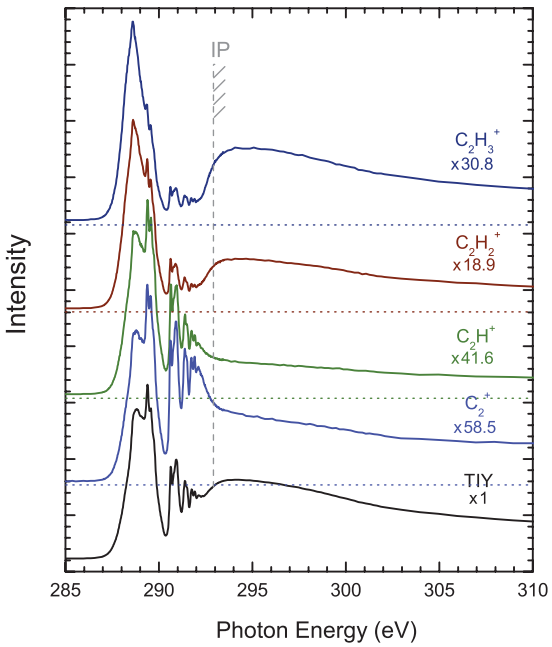

FIG. 3. Partial yields for $C_2H_3^+$, $C_2H_2^+$, C_2H^+, and C_2^+ ion fragments (cations) following photoexcitation of C_2H_4O near the C 1*s* ionization threshold, the TIY is added for comparison. Numerical values are approximate intensity values relative to the TIY at 295 eV.

The electronic structure of C_2H_4O has been elucidated in detail in the literature. There has been some controversy on the ordering of the valence energy levels according to the predictions of different calculations.[22–26] The electron configuration suggested by a many-body Green's function calculation,[24] which includes effects of electron correlation and reorganization, gives best overall agreement with the experimental ionization potentials[27] and therefore will be

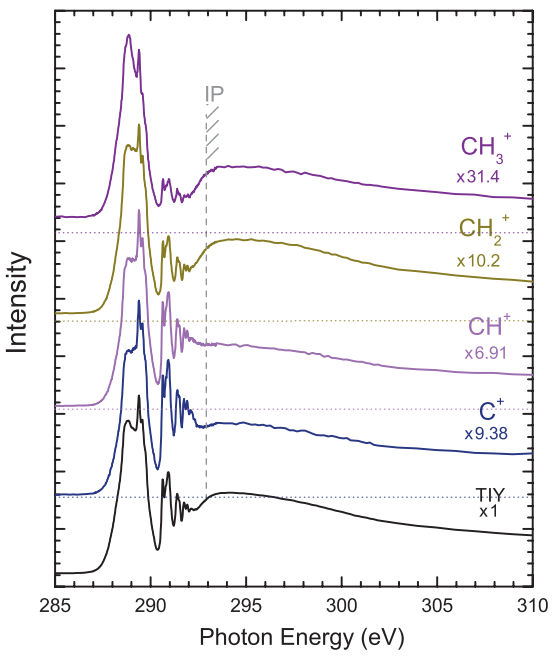

FIG. 4. Partial yields for CH_3^+, CH_2^+, CH^+, and C^+ ion fragments (cations) following photoexcitation of C_2H_4O near the C 1*s* ionization threshold. Numerical values are approximate intensity values relative to the TIY at 295 eV.

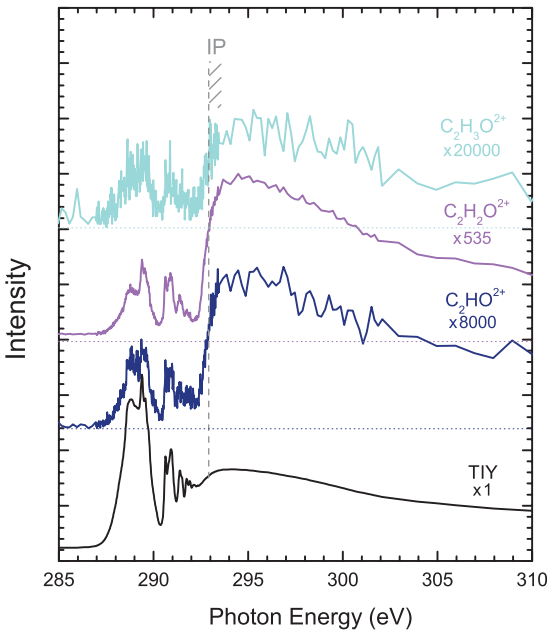

FIG. 5. Partial yields for $C_2H_3O^{2+}$, $C_2H_2O^{2+}$, and C_2HO^{2+} ion fragments (cations) following photoexcitation of C_2H_4O near the C 1*s* ionization threshold, the TIY is added for comparison. Numerical values are approximate intensity values relative to the TIY at 295 eV.

used as the basis for discussion in the present work. Accordingly, the ground state independent particle electronic configuration of ethylene oxide can be written as:

(i) Core orbitals (O 1*s* and C 1*s* core levels):

$$(1a_1)^2(2a_1)^2(1b_1)^2.$$

(ii) Occupied valence orbitals:

$$(3a_1)^2(4a_1)^2(2b_1)^2(1b_2)^2(5a_1)^2(3b_1)^2(1a_2)^2(6a_1)^2(2b_2)^2.$$

(iii) Unoccupied valence orbitals:

$$(7a_1)^0(4b_1)^0(8a_1)^0(3b_2)^0(5b_1)^0(2a_2)^0(6b_1)^0.$$

The characters of the valence orbitals from $2b_1$ in order of decreasing binding energy are σ_{CH2}, π_{CH2}, σ_{CC}, σ_{CO}, π_{CH2}, $(n_O, \sigma_{CO}, \sigma_{CC})$, and n_O, respectively. The $7a_1$ and $4b_1$ molecular orbitals (MOs) are predominantly of σ^*_{CO}, and $(\sigma^*_{CO}, \sigma^*_{CC})$ character, respectively, while the higher-lying levels have predominant Rydberg character.

ISEELS spectra have been reported for C_2H_4O around the C *K*-edge.[15] We use the same assignment to interpret our ion yield curves (see the TIY curve in Figs. 1–6). Namely, in the photon energy region 288–290 eV we assign the lowest-lying spectral features with maxima at 288.23 and 288.62 eV to transitions from the C 1*s* to the lowest-lying virtual orbitals $7a_1$ and $4b_1$, while the feature at 289.39 eV, with shoulders at 289.58 and 289.75 eV, is assigned to a transition to the 3*s* Rydberg state, better vibrationally resolved in our data set. Such vibrational spacing is consistent with a ring breathing or C–H stretching modes.[15] The higher photon energy region includes transitions to the other members of the Rydberg series, namely, 3*p* at 290.63 and 290.79 eV, 3*d* at 290.95 and 291.08 eV, 4*s* at 291.38 and 291.52, 4*p* at 291.75 eV, 4*d* at 291.91 eV, 5*s* at 292.08 eV, and 5*p* at 292.12 eV, converging to the ionization threshold at 292.91 eV.

A number of interesting experimental findings are evident from the comparison between the TIY and the partial ion yields for the various fragments. A first observation is the following: if we compare the total and the partial ion yields in a sequence of ion fragments corresponding to a subsequent fragmentation process, like the ones reported in Figs. 1–4, we notice immediately that the relative intensity of the spectral features related to transitions to the Rydberg series increases steadily while compared to the structures related to transitions to empty molecular orbitals. This effect has been reported by us in several other systems (see, e.g., Refs. 9 and 10) and it is explained by the nature of the final states reached after resonant Auger decay from core-excited states where the excited electron is promoted to a virtual orbital or to a Rydberg orbital, respectively. In the former case, the most likely decay processes are categorized as participator decay, leading to relatively long-lived one-hole valence final states, while when the primary excitation involves Rydberg states the system with one electron in an orbital far from the ionic core relaxes preferentially by spectator Auger decay and the singly charged ion with two valence holes and one electron on an outer diffuse orbital remains in excited states more susceptible to dissociation.

If we compare the ion yields for the doubly charged cations (Fig. 5), we can see, at least partially, the same effect,

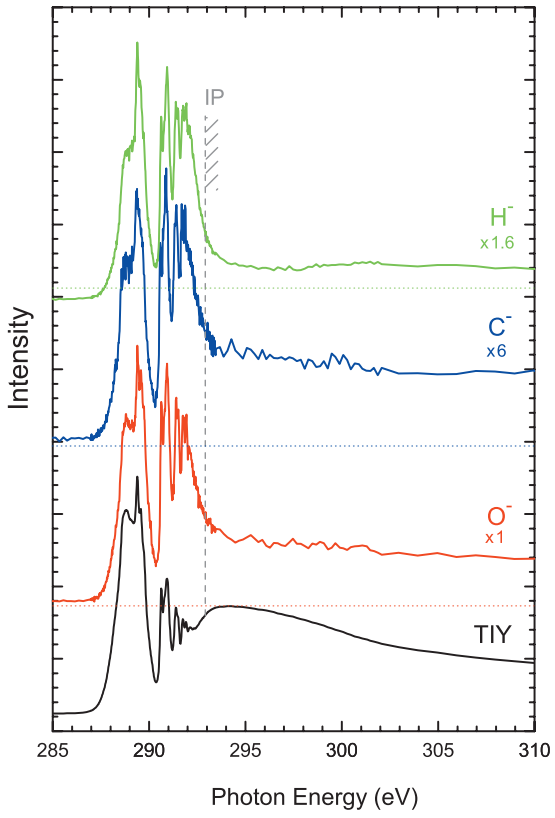

FIG. 6. Partial yields for H^-, C^-, and O^- negative ion fragments (anions) following photoexcitation of C_2H_4O near the C 1*s* ionization threshold, the TIY is added for comparison. Numerical values are approximate intensity values relative to the O-anion fragment at 295 eV.

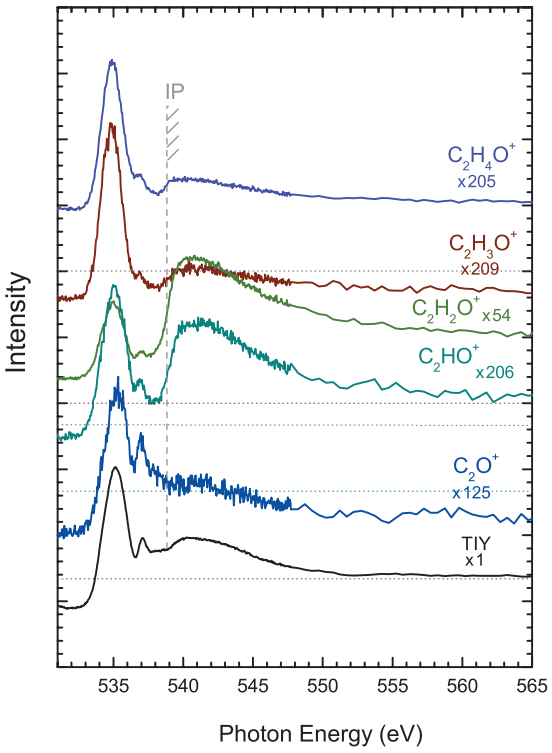

FIG. 7. Partial yields for $C_2H_4O^+$, $C_2H_3O^+$, $C_2H_2O^+$, C_2HO^+, and C_2O^+ ion fragments (cations) following photoexcitation of C_2H_4O near the O 1*s* ionization threshold, the TIY is added for comparison. Numerical values are approximate intensity values relative to the TIY at 555 eV.

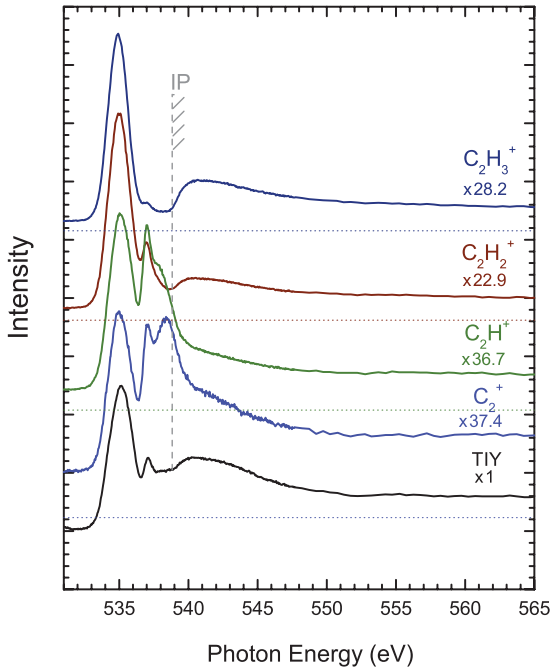

FIG. 8. Partial yields for $C_2H_3^+$, $C_2H_2^+$, C_2H^+, and C_2^+ ion fragments (cations) following photoexcitation of C_2H_4O near the O 1*s* ionization threshold, the TIY is added for comparison. Numerical values are approximate intensity values relative to the TIY at 555 eV.

but we also notice that the dominant feature is an increase in intensity at threshold, or threshold jump, which can be related to the transition from resonant Auger decay (taking place below threshold) to normal Auger decay above threshold; the production of doubly charged ionic species is dramatically increased when the final state already possesses two electron vacancies. A peculiar behavior is exhibited by the yield of the $C_2H_3O^{2+}$ fragment. This species has relatively low intensity above threshold compared to the other doubly charged ones (see Fig. 5), and furthermore in the $C_2H_3O^+$ yield shown in Fig. 1 there is very little intensity right above threshold, compared to the other fragments in the same series. It looks like both fragments with different total charge but the same number of C and H atoms are unstable right above threshold and undergo further fragmentation easily. The reason at the moment is unclear.

In Fig. 6 we report the ion yields for the three negatively charged species we could detect. The curves for the anions are similar, and they show some intensity above threshold, at variance with other smaller systems we investigated previously (see, e.g., Ref. 4). Above threshold the final states reached after normal Auger decay have two positive charges, and fragmentation processes leading to negatively charged species would imply a concentration of three positive charges on the partner fragments, which is unlikely in a relatively small molecule, but becomes more probable for larger systems. The production of negative ions above threshold could be connected to the presence of neutral doubly excited states, as we reported in several cases (see, e.g., Refs. 4 and 8), but in the present case no such processes are immediately evident.

Another interesting observation is that the anion production seems to be enhanced in the spectral region of the Rydberg states compared to that of the empty molecular orbitals. Again, this finding can be related to the dissociative behavior of the states reached after spectator decay: the extended fragmentation occurring after such processes can include channels producing not only positively charged but also negatively charged ions. Another factor to take into account is the possibility of radiative decay as alternative pathway for the Rydberg states, followed by creation of cation-anion pairs. However, for a molecule composed of light atoms this would be a minority channel and not likely to induce a strong effect.

B. C_2H_4O:O *K*-edge

We obtained TIY and partial ion yield spectra in the photon-energy region 525–570 eV, including the O 1*s* ionization threshold located at 538.84 eV. The energy scale has been calibrated according to,[20] and, like the C 1*s* region, agrees well with the electron energy loss measurements of Szel and Brion.[15] The list of positively charged fragments (cations) includes the singly charged species $C_2H_4O^+$, $C_2H_3O^+$, $C_2H_2O^+$, C_2HO^+, and C_2O^+, shown in Fig. 7, and $C_2H_3^+$, $C_2H_2^+$, C_2H^+, and C_2^+, shown in Fig. 8. The fragments CH_3O^+, CH_2O^+, CHO^+, CO^+, CH_3^+, CH_2^+, CH^+, C^+, H^+, H_2^+, H_3^+, O^+, OH^+, H_2O^+, C^{2+}, and O^{2+} are not shown because, like at the C *K* edge, they do not provide additional information. The negatively charged species (anions) H^-, C^-, and O^- also exhibit similar behavior as described for the C *K* edge, therefore, they too are not shown. In analogy with the C *K*-edge, the spectral assignment is the following: the features in the photon energy range 536–538 eV stem from an overlap of the transitions from the O 1*s* level to the two

lowest-lying molecular orbitals (535.16 eV) and the transition to the Rydberg 3*s* level (535.42 eV). The features at higher photon energy have a predominant Rydberg character (in particular the 3*d* Rydberg state at 537.07 eV).

Because below the O *K* edge the spacing between the excited states with valence character and those with Rydberg character is smaller than below the C *K* edge, the effect of a relative increase in the intensity of spectral features related to Rydberg transitions is less visible, although there is some enhancement for the peak at 537.07 eV (Rydberg 3*d*) as a function of progressive fragmentation in Fig. 7. The effect is more pronounced for the smaller fragments, as seen in Fig. 8.

An interesting effect which can be noticed in Fig. 8 for the yields of the lighter fragments, C_2H^+ and C_2^+, is the sudden drop in intensity at threshold, where the other yields shown exhibit an increase. Such an observation has been reported by several groups in atomic cases, and by us in CO (Ref. 5) and it is attributed to PCI effects: when core ionization of an atom or a molecule is induced close to threshold, a slow-moving photoelectron is ejected into the continuum. In the case of systems formed by light elements, the core-ionized state relaxes mainly through an Auger decay process and a fast Auger electron is released. If the Auger electron overtakes the photoelectron, energy and angular momenta can be exchanged. If the energy of the photoelectron is sufficiently small, it can be recaptured by the residual doubly charged ion (shakedown). The PCI effect has been relatively well studied and is relatively well understood for free atoms.[5] Few studies have been done on molecules,[28–30] based on electron or positive-ion spectroscopic measurements.

In Fig. 8 we observe that such recapture effect seems to be present in the yields of the two lighter fragments, while the two heavier ones do not show it. We can observe a similar effect for another small fragment, C_2O^+, in Fig. 7. All these fragments derive from an extended fragmentation of the doubly charged parent ion produced after Auger decay. We suggest the following: electron recapture occurs for the parent ion, and the recaptured electron ends up in a C–H antibonding orbital, inducing a breaking of one or more C–H bonds and leaving a singly charged fragment with one or no C–H bond. It is a rather speculative interpretation, but the peculiar spectral shape we observe is quite characteristic of the PCI effect.

The ion yields for the three negatively charged species (H^-, C^-, and O^-) in the O *K* region are similar to the C *K* observations, only much weaker in intensity (thus not shown here). As mentioned in the previous section, the major production for anions seems to be in the spectral region of the Rydberg states as compared to that of the empty molecular orbitals, and they show some small intensity above threshold.

C. C_2H_4S:C *K*-edge

The valence electronic structure of C_2H_4S has been investigated by He(I) and He(II) photoelectron spectroscopy.[27] The orbital ordering and composition are analogous to the C_2H_4O system, therefore we will assume that the same analogy holds for the virtual orbitals, for which no data are available. There are also no literature data on the absorption of C_2H_4S around the C *K*-edge, therefore we obtained some partial yield curves for some fragments to perform a spectral assignment in analogy with the C_2H_4O results.

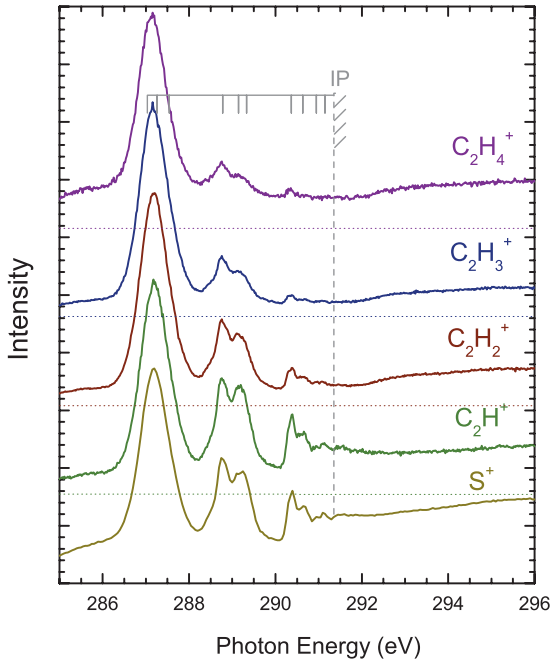

FIG. 9. Partial yields for $C_2H_4^+$, $C_2H_3^+$, $C_2H_2^+$, C_2H^+, and S^+ ion fragments (cations) following photoexcitation of C_2H_4S near the C 1*s* ionization threshold. The spectra are normalized on the transition near 287.2 eV.

In Fig. 9 we show the partial yield curves for some of the fragments we collected in the photon-energy region including the C 1*s* photoionization threshold. The general appearance of the yield curves is very similar to the oxygenated analog (see Figs. 1–4), therefore in Table I, we adopt a similar spectral assignment. Namely, the first spectral feature with maximum at 287.2 eV includes the transitions from the C 1*s* level to the two lowest-lying virtual orbitals, with an overlapping transition to the 4*s* Rydberg level. The following spectral features at 288.77, 289.09, 289.27, 290.37, 290.65, 290.08, and 291.15 eV correspond to transitions to levels with pure Rydberg character (4*p*, 4*d*, 5*s*, 5*p*, and 5*d*, in anal-

TABLE I. A simplifed spectral assignment and observed energies for excitation of C 1*s* electrons in C_2H_4S.

Assignment $C(1s^{-1})\rightarrow$	Present measurement (eV)
$a_1, b_1, 4s$	287.2 ± 0.003
$4p$	288.77 ± 0.01
$4d$	289.09 ± 0.01
$4d$	289.27 ± 0.03
$5s$	290.37 ± 0.02
$5s$	290.65 ± 0.05
$5p$	291.08 ± 0.01
$5d$	291.14 ± 0.05
IP[a]	291.15 ± 0.2
⋯	295.48 ± 0.09
⋯	300.29 ± 0.19

[a]Ionization threshold was estimated from the vertical ionization threshold located at 291.85 ± 0.05.

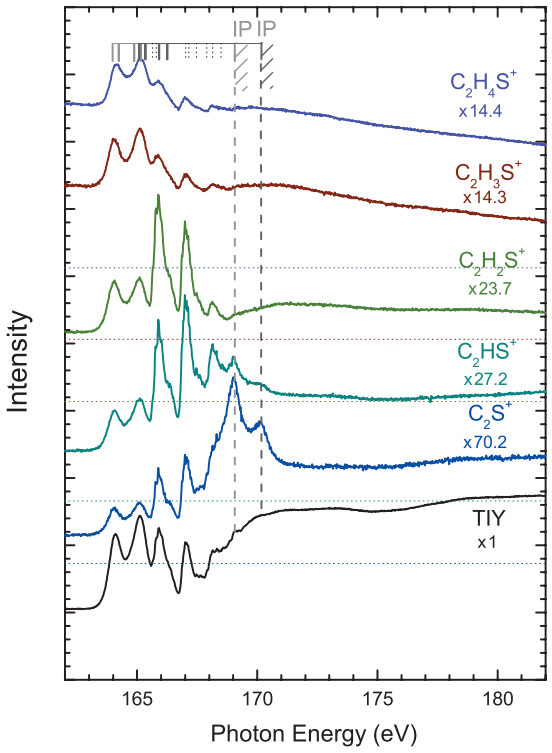

FIG. 10. Partial yields for $C_2H_4S^+$, $C_2H_3S^+$, $C_2H_2S^+$, C_2HO^+, and C_2S^+ ion fragments (cations) following photoexcitation of C_2H_4S near the S $2p$ ionization thresholds, the TIY is added for comparison. Numerical values are approximate intensity values relative to the TIY at 173 eV.

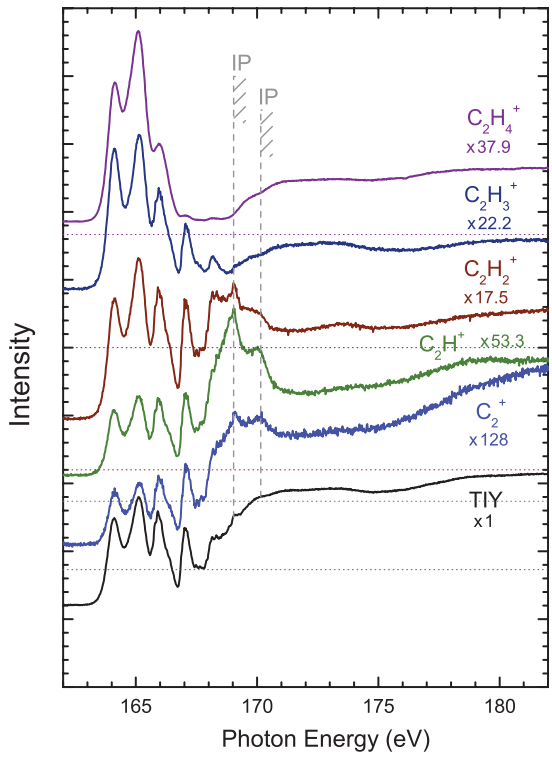

FIG. 11. Partial yields for $C_2H_4^+$, $C_2H_3^+$, $C_2H_2^+$, C_2H^+, and C_2^+ ion fragments (cations) following photoexcitation of C_2H_4S near the S $2p$ ionization thresholds, the TIY is added for comparison. Numerical values are approximate intensity values relative to the TIY at 173 eV.

ogy with C_2H_4O). The vertical ionization threshold, 291.85 eV, was placed by taking the derivative of the $C_2H_2S^+$ ion yield (spectrum not shown here) between 290 and 293 eV, and fitting the resulting peak with a Gaussian. Estimating from the full width at half maximum of this Gaussian, the adiabatic ionization threshold should be located near 291.15 eV, which agrees well to the shape of the other ion yield curves. We do not assign the above threshold peaks located at 295.48 and 300.29 eV. These assignments are confirmed by the previously discussed effect that the relative intensities of states with pure Rydberg character increase as a function of the extended fragmentation, and an increase in relative intensity for the peaks around 288–291 eV can clearly be observed as the fragmentation increases.

An alternative assignment compatible with the described effect would place the Rydberg 4*s* transition at 288.7 eV, and shift the other Rydberg states accordingly. The term value for the Rydberg 4*s* would then be 2.7 eV, while for C_2H_4O it is 3.45 eV. However, the term value for the Rydberg 3*p* in C_2H_4O is 2.19, while for this alternative assignment in C_2H_4S it would be 2.2. Therefore we prefer the first assignment, which is also more consistent with the results obtained at the S $L_{2,3}$-edge (see discussion below).

D. C_2H_4S:S $L_{2,3}$-edge

We detected a wealth of fragments in the photon energy region including the S $2p$ ionization thresholds. The positive singly charged ions are $C_2H_4S^+$, $C_2H_3S^+$, $C_2H_2S^+$, C_2HS^+, and C_2S^+, shown in Fig. 10, and $C_2H_4^+$, $C_2H_3^+$, $C_2H_2^+$, C_2H^+, and C_2^+, shown in Fig. 11. The fragments CH_4S^+, CH_3S^+, CH_2S^+, CHS^+, CS^+, H^+, H_2^+, H_3^+, CH_3^+, CH_2^+, CH^+, C^+, SH_4^+, SH_3^+, SH_2^+, and SH^+ were measured but are not presented here because they do not provide further information by being either similar to other partial ion yields or because they simply mimic the TIY. The positive doubly charged species are $C_2H_3S^{2+}$, $C_2H_2S^{2+}$, C_2HS^{2+}, CHS^{2+}, and CS^{2+}, shown in Fig. 12. Among the other detected cations, an interesting comparison can be made between the ion yield curves of S^+, S^{2+}, and S^{3+}, shown in Fig. 13. The only detected negatively charged species are C^- and S^-, with rather low intensity; they are therefore not shown because, like C_2H_4O, the major production for anions seems to be in the spectral region of the Rydberg states.

Because there are no literature data on absorption of C_2H_4S around the S $L_{2,3}$-edge, in Table II, we propose a tentative assignment based on the one suggested earlier in this paper for the C *K* edge. The main difference is that since the S $2p$ level is spin-orbit split we expect a doubling of the spectral features as compared to the C *K* edge. Therefore the proposed assignment is the following: the three peaks at 163.98, 164.24, and 165.09 eV correspond to transitions to the first two virtual molecular orbitals of a_1 and b_1 symmetry, in analogy with C_2H_4O.[15] Using the previous argument on the relative intensities of spectral features related to transitions to virtual orbitals or Rydberg levels, the relative intensity changes in Figs. 10 and 11 confirm the assignment. In particular, we can attribute the intense peak at 164.88 eV in the ion yield curves (e.g., of C_2HS^+ in Fig. 10 and C_2H^+ in Fig. 11) as related to the 4*s* Rydberg state in the series con-

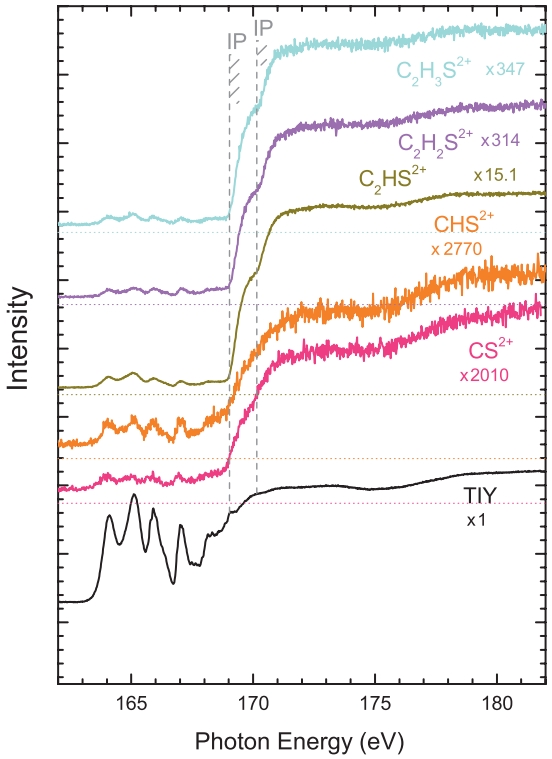

FIG. 12. Partial yields for $C_2H_3S^{2+}$, $C_2H_2S^{2+}$, C_2HS^{2+}, CHS^{2+}, and CS^{2+} ion fragments (cations) following photoexcitation of C_2H_4S near the S $2p$ ionization thresholds, the TIY is added for comparison. Numerical values are approximate intensity values relative to the TIY at 173 eV.

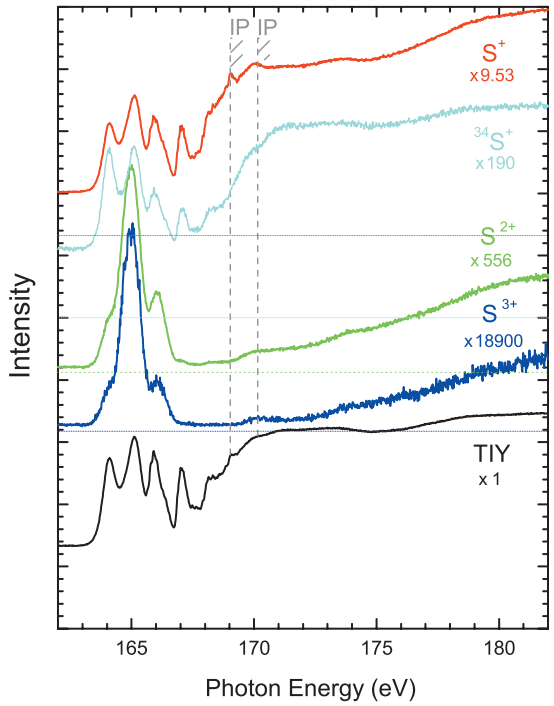

FIG. 13. Partial yields for S^+, S^{2+}, and S^{3+} ion fragments (cations) following photoexcitation of C_2H_4S near the S $2p$ ionization thresholds, the TIY is added for comparison. Numerical values are approximate intensity values relative to the TIY at 173 eV.

verging to the S $2p_{3/2}$ threshold, because it appears in the ion yield of the lighter fragments at a photon energy lower than the peak at 165.16 eV, which most likely corresponds to the S $2p_{1/2} \rightarrow b_2$ transition.

A detailed assignment of all members of the Rydberg series would be rather speculative; therefore we suggest only a general attribution to transitions to either virtual orbitals or Rydberg levels. We can assign with certainty the intense peaks at 165.92 eV as the $4s$ and 166.26 as b_2 of the series converging to the S $2p_{1/2}$, mainly on the observation that they show an energy separation with respect to the peak at 165.16 and 165.35 eV compatible with the spin-orbit splitting (see the discussion on Fig. 12). We do not assign the peaks located at 165.65, 165.80, 167.03, 167.15, 167.47, 167.90, 168.14, and 168.50 eV, the assignment of which would require detailed theoretical calculations. If we examine the yields for the lighter ion fragments in Figs. 10 and 11, for instance C_2S^+, we notice a sudden decrease in signal immediately above the ionization threshold. We previously discussed this effect for the C_2H_4O system (see in Fig. 8). Similar considerations apply, and we therefore attribute this trend to PCI effects, which seems to be more important for more extended fragmentation.

The doubly charged species shown in Fig. 12 mainly show a large increase in intensity when crossing the ionization thresholds, due to the creation of doubly charged ions following normal Auger decay. We therefore used them to estimate the energy positions of the two adiabatic ionization thresholds at 169.07 and 170.18 eV, from the vertical ionization thresholds at 169.28 and 170.39 eV, resulting in a spin-orbit splitting for the S $2p$ levels of 1.11 eV. The vertical ionization thresholds were placed by taking the derivative of the C_2HS^{2+} ion yield between 168 and 172 eV, and fitting the resulting two peaks with Gaussians.

In Fig. 13 we compare three positively charged fragments whose ion yields are particularly interesting, namely, S^+, S^{2+}, and S^{3+}. We also show another ion yield for a weak

TABLE II. Tentative spectral assignment and observed energies for excitation of S $2p$ electrons in C_2H_4S.

Assignment $S(2p^{-1})\rightarrow$	Present measurement (eV)
$(2p_{3/2}^{-1})a_1$	163.98 ± 0.003
$(2p_{3/2}^{-1})b_1$	164.24 ± 0.005
$(2p_{3/2}^{-1})4s$	164.88 ± 0.007
$(2p_{1/2}^{-1})a_1$	165.09 ± 0.01
$(2p_{3/2}^{-1})b_2$	165.16 ± 0.01
$(2p_{3/2}^{-1})b_1$	165.35 ± 0.01
⋯	165.65 ± 0.01
⋯	165.8 ± 0.01
$(2p_{1/2}^{-1})4s$	165.92 ± 0.01
$(2p_{1/2}^{-1})b_2$	166.26 ± 0.01
⋯	167.03 ± 0.005
⋯	167.15 ± 0.05
⋯	167.47 ± 0.05
⋯	167.90 ± 0.05
⋯	168.14 ± 0.05
⋯	168.50 ± 0.05
$(2p_{3/2}^{-1})$IP[a]	169.07 ± 0.1
$(2p_{1/2}^{-1})$IP[a]	170.18 ± 0.15

[a]Ionization thresholds have been estimated from the vertical ionization thresholds located at 169.28 ± 0.005 and 170.39 ± 0.01.

fragment of mass/charge 17, which could correspond to SH_2^{2+}. However, the ^{34}S isotope has an abundance of 4.2%,[31] therefore this fragment is likely to correspond to $^{34}S^{2+}$, as hinted at by the similarity of its yield with that of S^{2+}. Furthermore, we do not detect either mass/charge 16.5, corresponding to SH^{2+}, or mass/charge 17.5, corresponding to SH_3^{2+}, which should be present together with SH_2^{2+}.

We can immediately observe that the S^+ and S^{2+} yields are very different, implying that they derive from two different fragmentation processes, and not from a second-step Auger decay of the singly charged species. This argument can be clarified by comparing the yields for S^{2+} and S^{3+}, which are similar and clearly hint at a subsequent electron emission from the doubly charged fragment. Another striking finding is that in the S^{2+} yield the Rydberg series is suppressed, and furthermore the relative intensity of the residual three peaks, corresponding to transitions from the S $2p$ spin-orbit split levels to the two lowest-lying virtual orbitals (see above discussion) exhibit a very different intensity ratio while compared to the majority of the other yield curves. In particular, the transition to the virtual orbital of a_1 symmetry has much lower probability than the one with b_1 symmetry.

To interpret this finding, we need to briefly summarize the nature and fragmentation probabilities of the valence final states reached after resonant Auger decay. We discussed in previous sections that participator decay, more probable after excitation to virtual molecular orbitals, which are in general less diffuse than Rydberg levels, leads to relatively long-lived one-hole valence final states. In contrast, spectator Auger decay, more probable after excitation to Rydberg states, leads to a singly charged ion with two valence holes and one electron in an outer diffuse orbital. This type of two-hole one-particle ionic state is more susceptible to dissociate than the one-hole states formed from participator decay. Based on this argument, it looks like S^{2+} is mostly produced by fragmentation following participator decay, since features related to the Rydberg series are not present in its yield, at variance with the S^+ yield where such peaks are clearly visible.

The nature of the participator decay leading directly to S^{2+} remains to be explained. We make the following hypothesis: the direct production of a doubly charged fragment can stem from a valence doubly charged molecular state. If some of the states reached after participator decay are above the double ionization threshold, they can fragment by directly producing a doubly charged fragment. Furthermore, electron vacancies localized on the S atom are likely to occur, because the highest occupied valence orbital (HOMO) has S lone-pair character. Therefore we assume that S^{2+} is created by fragmentation of a doubly charged molecular state with two electron vacancies on the S site. This assignment is strengthened by the observation that S^{2+} is more abundant following the excitation to the second virtual orbital. A higher amount of total energy is then put into the system, and the states reached after electron decay above the double ionization threshold should be more numerous. A similar argument was used in partial ion yield experiments in water below the O K edge to explain the higher production of the H^+ fragment at the second transition, at higher photon energy compared to the transition to the lowest unoccupied molecular orbital.[32]

IV. CONCLUSION

We performed partial and TIY experiments to shed light on the photofragmentation patterns of two three-membered ring heterocyclic molecules, C_2H_4O and C_2H_4S. The ionization edges investigated include the C $1s$ and O $1s$ thresholds in C_2H_4O, and the S $2p$ and C $1s$ thresholds in C_2H_4S. We propose a new assignment of the spectral features around the C K edge and the sulfur $L_{2,3}$ edges in C_2H_4S, for which no previous literature data were reported. In both molecules, we observe high fragmentation efficiency leading to positive and negative ions when exciting these molecules along resonances involving core-to-Rydberg transitions. A state-selective fragmentation pattern is analyzed in C_2H_4S which leads to the direct production of S^{2+}, and we describe it in terms of decay of excitations to virtual orbitals to final states above the double-ionization threshold.

ACKNOWLEGEMENTS

The authors thank the staff of the ALS for their excellent support. Support from the National Science Foundation under NSF Grant No. PHY-05-55699 is gratefully acknowledged. M.N.P. thanks the Wenner-Gren Stiftelse for a grant to support her stay at the ALS. This work was performed at the Advanced Light Source, which is supported by DOE (Grant No. DE-AC03-76SF00098).

[1] I. Nenner and P. Morin, in *VUV and Soft X-Ray Photoionization*, edited by U. Becker and D. A. Shirley (Plenum, New York, 1996), p. 291.
[2] J. Kikuma and B. P. Tonner, J. Electron Spectrosc. Relat. Phenom. **82**, 41 (1996).
[3] S.-Y. Chen, C.-I. Ma, D. M. Hanson, K. Lee, and D. Y. Kim, J. Electron Spectrosc. Relat. Phenom. **93**, 61 (1998).
[4] W. C. Stolte, D. L. Hansen, M. N. Piancastelli, I. Dominguez Lopez, A. Rizvi, O. Hemmers, H. Wang, A. S. Schlachter, M. S. Lubell, and D. W. Lindle, Phys. Rev. Lett. **86**, 4504 (2001).
[5] D. L. Hansen, W. C. Stolte, O. Hemmers, R. Guillemin, and D. W. Lindle, J. Phys. B **35**, L381 (2002), (and references therein).
[6] G. Öhrwall, M. M. Sant'Anna, W. C. Stolte, I. Dominguez Lopez, L. T. N. Dang, A. S. Schlachter, and D. W. Lindle, J. Phys. B **35**, 4543 (2002).
[7] W. C. Stolte, G. Öhrwall, M. M. Sant'Anna, I. Dominguez Lopez, L. T. N. Dang, M. N. Piancastelli, and D. W. Lindle, J. Phys. B **35**, L253 (2002).
[8] S.-W. Yu, W. C. Stolte, G. Öhrwall, R. Guillemin, M. N. Piancastelli, and D. W. Lindle, J. Phys. B **36**, 1255 (2003).
[9] M. N. Piancastelli, W. C. Stolte, G. Öhrwall, S.-W. Yu, D. Bull, K. Lantz, A. S. Schlachter, and D. W. Lindle, J. Chem. Phys. **117**, 8264 (2002).
[10] D. Céolin, M. N. Picancastelli, R. Guillemin, W. C. Stolte, S.-W. Yu, O. Hemmers, and D. W. Lindle, J. Chem. Phys. **126**, 084309 (2007).
[11] H. L. Kim, S. Satyapal, P. Brewer, and R. Bersohn, J. Chem. Phys. **91**, 1047 (1989).
[12] F. Qi, O. Sorkhabi, and A. G. Suits, J. Chem. Phys. **112**, 10707 (2000).
[13] F. Qi, O. Sorkhabi, A. G. Suits, S.-H. Chien, and W.-K. Li, J. Am. Chem. Soc. **123**, 148 (2001).
[14] S.-Y. Chiang and Y.-S. Fang, J. Electron Spectrosc. Relat. Phenom. **144–147**, 223 (2005).
[15] K. H. Szel and C. E. Brion, J. Electron Spectrosc. Relat. Phenom. **57**, 117 (1991).
[16] E. Hudson, D. A. Shirley, M. Domke, G. Remmersand, and G. Kaindl, Phys. Rev. A **49**, 161 (1994).
[17] R. Guillemin, W. C. Stolte, S.-W. Yu, and D. W. Lindle, J. Chem. Phys. **122**, 094318 (2005).

[18] K. C. Prince, L. Avaldi, M. Coreno, R. Camilloni, and M. de Simone, J. Phys. B **32**, 2551 (1999).
[19] M. Tronc, G. C. King, and F. Read, J. Phys. B **12**, 145102 (1979).
[20] M. Domke, T. Mandel, A. Puschmann, C. Xue, D. A. Shirley, G. Kaindl, H. Petersen, and P. Kuske, Rev. Sci. Instrum. **63**, 80 (1992).
[21] W. C. Stolte, R. Guillemin, S.-W. Yu, and D. W. Lindle, J. Phys. B **41**, 145102 (2008).
[22] H. Basch, M. B. Robin, N. A. Kuebler, C. Baker, and D. W. Turner, J. Chem. Phys. **51**, 52 (1969).
[23] P. D. Mollere and K. N. Houk, J. Am. Chem. Soc. **99**, 3226 (1977).
[24] W. von Niessen, L. S. Cederbaum, and W. P. Kraemer, Theor. Chim. Acta **44**, 85 (1977).
[25] K. Kimura, S. Katsumata, Y. Achiba, T. Yamazaki, and S. Iwata, *Handbook of He (I) Photoelectron Spectra of Fundamental Organic Molecules* (Japan Scientific Societies, Tokyo, 1981).
[26] G. De Alti, P. Decleva, and A. Lisini, J. Mol. Struct.: THEOCHEM **108**, 129 (1984).
[27] A. Schweig and W. Thiel, Chem. Phys. Lett. **21**, 541 (1973).
[28] D. L. Hansen, G. B. Armen, M. E. Arrasate, J. Cotter, G. R. Fischer, K. T. Leung, J. C. Levin, R. Martin, P. Neill, R. C. C. Perera, I. A. Sellin, M. Simon, Y. Uehara, B. Vanderford, S. B. Whitfield, and D. W. Lindle, Phys. Rev. A **57**, R4090 (1998).
[29] M. K. Odling-Smee, E. Sokell, A. A. Wills, and P. Hammond, J. Phys. B **32**, 2529 (1999).
[30] G. Dujardin, L. Hellner, B. J. Olsson, M. J. Besnard-Ramage, and A. Dadouch, Phys. Rev. Lett. **62**, 745 (1989).
[31] J.R. De Laeter, J. K. Böhler, P. De Bièvre, H. Hidaka, H.S. Peiser, K.J. R. Rosmani and P.D. P. Taylor, Pure Appl. Chem. **75**, 683 (2003), and references therein.
[32] M. N. Piancastelli, F. Heiser, A. Hempelmann, O. Gessner, A. Rëdel, and U. Becker, Phys. Rev. A **59**, 300 (1999).